

Channel modeling for underwater scattered light communication based on Gaussian and Bessel beams

Yi Gao (高翼), Zhitong Huang (黄治同)*, Jie Xu (徐杰), Hongcheng Qiu (邱宏成), Yan Jia (贾晏), and Yuefeng Ji (纪越峰)

State Key Laboratory of Information Photonics and Optical Communications, School of Information and Communication Engineering, Beijing University of Posts and Telecommunications, Beijing 100876, China

*Corresponding author: hzt@bupt.edu.cn

Received July 17, 2024 | Accepted January 21, 2025 | Posted Online May 30, 2025

Underwater scattered light communication (USLC) utilizes the strong scattering properties of seawater to achieve a non-line-of-sight (NLOS) communication channel, which is a promising solution to the stringent alignment requirements and random transmission path blocking in underwater wireless optical communication. In this Letter, we model the channel for USLC based on Gaussian and Bessel beams, in which we comprehensively explore the effects of different water types and transceiver configurations on USLC and simulate the photon propagation in seawater by Monte Carlo (MC) method. Specifically, we analyze the fluctuation in received signal strength as a function of the communication distance across three distinct water types, in which the model considers the influence of different optical wavelengths and spatial modes at the transmitter as well as various optical lens configurations at the receiver. Modeling and experiments validate blue Gaussian beams for short-range, low-turbidity cases; green Bessel beams for long-range, high-turbidity conditions; and the receiver antenna's utility which is restricted to short-range applications. The conclusion obtained can be used for the selection of transceiver devices in USLC systems.

Keywords: underwater scattered light communication; Gaussian beam; Bessel beam; channel model.

DOI: [10.3788/COL202523.060606](https://doi.org/10.3788/COL202523.060606)

1. Introduction

With the deepening of marine development, the escalating volume of data transmission highlights the imperative for low-cost and high-rate underwater wireless communication technology. Compared to conventional underwater acoustic and radio frequency communication, underwater wireless optical communication (UWOC) is emerging as a highly competitive solution, distinguished by its superior attributes of higher bandwidth, lower latency, reduced cost, and power consumption^[1].

A major obstacle to the widespread adoption of UWOC is its strict alignment requirement between transceivers. UWOC equipment usually relies on underwater vehicles for levitation and movement, which is prone to beam shifts due to equipment vibrations and water disturbances. Seawater turbulence can also cause beam misalignment and spot distortion^[2]. In addition, obstacles such as fish and plants pose significant challenges in establishing a reliable line-of-sight (LOS) link.

To address these challenges, underwater scattered light communication (USLC) utilizing non-line-of-sight (NLOS) links provides a feasible solution, with established theoretical studies and experiments confirming its efficiency^[3-6].

At Lake Boyarskoe, Russian researchers experimentally determined that the maximum base distances of the green and blue laser beams of the USLC system were, respectively, 40 and 20 m^[4]. Mohammed *et al.* demonstrated that USLC was robust to turbulence induced by bubbles, temperature gradients, and salinity gradients^[5,6].

Accurate channel modeling is critical for effectively evaluating the performance of USLC systems^[7-9]. Sun *et al.* demonstrated in the laboratory that smaller azimuths, stronger water turbidity, and shorter wavelengths could reduce path loss in the 35-cm range^[7]. Umar *et al.* modeled the temporal dispersion of USLC in coastal and harbor water environments^[8]. Boluda-Ruiz *et al.* modeled scattering communications and analyzed the effect of the receiver field-of-view (FOV) angle when using LEDs and LDs^[9].

However, the above studies exhibit a limitation in their analysis of factors influencing the scattering channel, ignoring the equally significant impact of the spatial distribution of the transmitter beam and the receiver's optical antenna on the performance of USLC systems. Therefore, in this Letter, we establish a more comprehensive composite USLC channel model based on the Monte Carlo (MC) method and investigate the effects

of seawater turbidity, communication distance, and transceiver configuration on the USLC performance. The reliability of the model is verified experimentally.

2. Composite Channel Modeling for USLC

The USLC channel model is affected by the combination of the transmitter, the receiver, and the water quality, clearly distinguishing it from LOS UWOC and NLOS UWOC, which relies on interface reflections to propagate signals. Considering random behaviors such as particle distribution and photon scattering, the MC method is well suited to handle such scenarios. Figure 1 shows the flowchart of the channel modeling using the MC method, simulating the process of photons from excitation to reception by a receiver. Throughout the simulation, computational efficiency is maintained by specifying that photons are considered quenched as soon as they exceed a predefined spatial boundary or their intensity decays below a critical threshold.

2.1. Modeling of emitted light for Gaussian and Bessel beams

It is valuable to study the effect of the spatial pattern of the transmitter beam on the USLC due to the differences in the transmission performance of beams with different spatial patterns under the effects of seawater absorption, scattering, and turbulence^[10,11].

For a Gaussian beam, according to the transverse intensity distribution formula and the Box–Muller transformation method, the polar coordinates (r, α) of the photon in the x - y plane, as shown in Fig. 2(a), can be expressed as

$$\begin{cases} r = \omega_0 \sqrt{-(\ln R_1)/2} \\ \alpha = 2\pi R_2 \end{cases}, \quad (1)$$

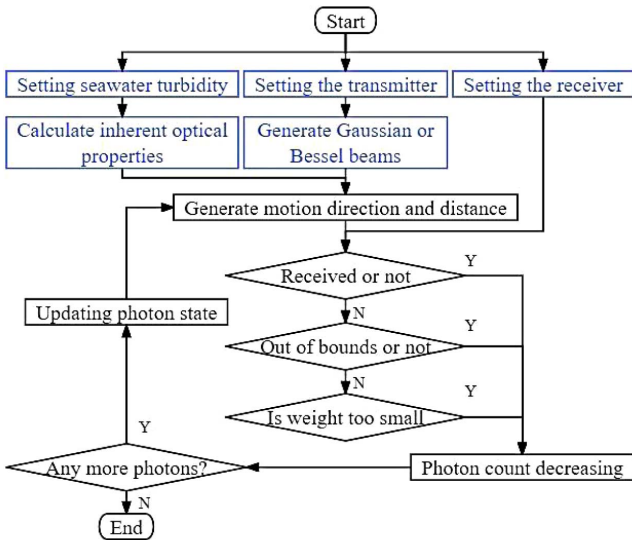


Fig. 1. MC algorithm flowchart.

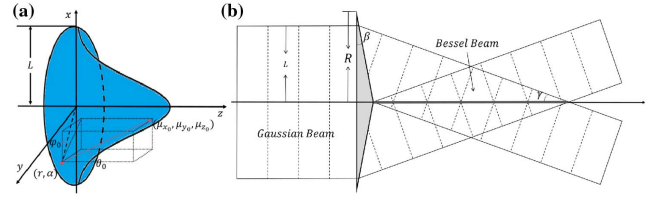


Fig. 2. (a) Photon initialization for Gaussian beams. (b) Generation of Bessel beams using the axial cone lens.

where ω_0 represents the beam waist radius, and R_1 and R_2 denote the samples of uniform distribution $U(0, 1)$.

Assuming that the divergence half-angle of the beam is δ and considering the radial symmetry of the beam, the divergence angle θ_0 and azimuth angle φ_0 of each photon can be expressed as

$$\begin{cases} \theta_0 = \delta R_3 \\ \varphi_0 = 2\pi R_4 \end{cases}, \quad (2)$$

where $R_3, R_4 \sim U(0, 1)$.

Therefore, the initial position (x_0, y_0, z_0) and the motion direction $(\mu_{x_0}, \mu_{y_0}, \mu_{z_0})$ of a photon can be expressed as

$$\begin{cases} (x_0, y_0, z_0) = (r \cos \alpha, r \sin \alpha, 0) \\ (\mu_{x_0}, \mu_{y_0}, \mu_{z_0}) = (\cos \varphi_0 \sin \theta_0, \sin \varphi_0 \sin \theta_0, \cos \theta_0) \end{cases}. \quad (3)$$

For a Bessel beam, it is usually generated by passing a parallel Gaussian beam through an axial cone lens, as shown in Fig. 2(b). The non-diffracting property of the Bessel beams allows them to maintain intensity distribution during propagation, which concentrates energy in a smaller area and enables longer-distance transmission. Additionally, the self-repairing property enables them to recover the original intensity distribution after encountering obstacles such as bubbles, demonstrating robustness against complex underwater environments. Therefore, compared to Gaussian beams, Bessel beams are more suitable for channel environments in long-range UWOC^[11].

When a parallel beam enters the axial cone lens, it is refracted into a conical wave, which then interferes during propagation and generates a zero-order Bessel beam in the rhombus region. Since the beam enters the axial cone lens perpendicular to the bottom, refraction occurs only on the conical surface. The position and direction of the photon as it leaves the axial cone lens can be calculated as

$$\begin{cases} (x_0, y_0, z_0) = (r \cos \alpha, r \sin \alpha, (R - r) \tan \beta) \\ \mu_{x_0} = \cos \alpha \sin \beta (\sqrt{1 - n^2 \sin^2 \beta} - n \cos \beta) \\ \mu_{y_0} = \sin \alpha \sin \beta (\sqrt{1 - n^2 \sin^2 \beta} - n \cos \beta) \\ \mu_{z_0} = n \sin^2 \beta + \cos \beta \sqrt{1 - n^2 \sin^2 \beta} \end{cases}, \quad (4)$$

where R and β , respectively, denote the base radius and base angle of the lens, and $n = n_0/n_1$ denotes the relative refractive index of the air to the lens.

2.2. Modeling of photon propagation based on seawater turbidity and optical wavelengths

The propagation of photons is determined by the intrinsic optical properties (IOPs) of seawater, which are determined by seawater's composition and are wavelength-selective. As the beam light propagates, photons interact with particles in the seawater, resulting in either energy attenuation due to absorption or a change in direction due to scattering. The former is described by the absorption coefficient and the latter by the volume scattering function (VSF). Both can derive other IOPs.

Petzold *et al.* proposed a method of simulating seawater in the laboratory using Maalox, suggesting that by altering the concentration of the Maalox solution^[12], different aquatic environments can be simulated^[13]. The absorption coefficient a of the seawater can be expressed as^[14]

$$a(\lambda) = a_w(\lambda) + 0.198 \exp[-0.01(\lambda - 440)]C_M, \quad (5)$$

where $a_w(\lambda)$ is the absorption coefficient of the pure seawater, and C_M is the concentration of the Maalox in mg/L.

The VSF describes the angular distribution of the scattered light in the water column, and its selection plays a crucial role in the accuracy of simulation results. Optical oceanography researchers have developed instruments to measure the VSF, obtained measurements from real ocean environments, and proposed fitting functions,

$$p(\lambda, \theta) = b_w(\lambda)p_w(\theta) + b_M(\lambda)p_M(\theta)C_M, \quad (6)$$

where $b_w(\lambda)$ and $b_M(\lambda)$ are the scattering coefficients of the pure seawater and the Maalox, respectively. $p_w(\theta)$ and $p_M(\theta)$ are the scattering phase functions of the pure seawater and the Maalox, respectively^[15].

The probability of photon scattering is determined by the turbidity of the water, and the distance between successive scattering events is stochastic. Therefore, the path length of a photon can be expressed as^[16]

$$s = -\frac{\ln R}{c(\lambda)}, \quad (7)$$

where $c(\lambda)$ is the attenuation coefficient, which can represent the turbidity of the seawater.

After the photon moves s distance, its position is updated as

$$(x', y', z') = (x, y, z) + (\mu_x, \mu_y, \mu_z)s. \quad (8)$$

Photons lose energy due to absorption by particles in the water,

$$w_i = w_{i-1}e^{-as}, \quad (9)$$

where w_i is the weight at the occurrence of the i th scattering. Once the photon's energy falls below the threshold (set at 10^{-8}), it is considered too weak to continue tracking.

Collisions between photons and particles are considered elastic collisions, resulting in only direction changes without power loss. The direction change is defined as^[17]

$$\begin{cases} \mu'_x = \frac{\sin \theta (\mu_x \mu_z \cos \varphi - \mu_y \sin \varphi)}{\sqrt{1 - \mu_z^2}} + \mu_x \cos \theta \\ \mu'_y = \frac{\sin \theta (\mu_y \mu_z \cos \varphi - \mu_x \sin \varphi)}{\sqrt{1 - \mu_z^2}} + \mu_y \cos \theta \\ \mu'_z = -\sin \theta \cos \varphi \sqrt{1 - \mu_z^2} + \mu_z \cos \theta, |\mu_z| \leq 1 - eps \end{cases}, \quad (10)$$

$$\begin{cases} \mu'_x = \cos \varphi \sin \theta \\ \mu'_y = \sin \varphi \sin \theta \\ \mu'_z = \text{sign}(\mu_z) \cos \theta, |\mu_z| > 1 - eps \end{cases}, \quad (11)$$

where the value of θ is determined by the VSF and $\varphi \sim U(0, 2\pi)$.

2.3. Modeling of receiver optical antenna

The optical antenna and photodetector of the receiver determine its FOV and photosensitive area, which affects the received optical power. The optical antenna can effectively enhance the received optical power in LOS communication based on direct light and NLOS communication based on reflected light. In both schemes, the received photons are concentrated near the main optical axis and move in relatively the same direction. However, in USLC, there are huge differences in the motion direction of the received photons due to the randomness of the particle distribution and photon scattering. Therefore, it is necessary to investigate whether the optical antenna of the receiver can realize power gain at USLC.

In the case of a lens, the most commonly used optical antenna, it limits the FOV of the receiver in increasing the equivalent photosensitive area according to the limit of étendue^[18]. The maximum optical gain of a lens with refractive index n as a function of FOV can be expressed as

$$C_{\max}(\eta) = \frac{n^2}{\sin^2 \eta}, \quad (12)$$

where η is half of the FOV.

The total power of the received photons can be expressed as

$$\omega = \sum_{m=1}^n \omega_m, \quad (13)$$

$$\begin{cases} p_m \in C_{\max}(\eta)S \\ \langle -d_m, N \rangle < \eta \end{cases}, \quad (14)$$

where p_m is the photon position, d_m is the photon's direction vector, S is the light-sensitive region of the receiver without the lens, and N is the normal vector of the receiving surface.

Neglecting the saturation power limitations of the receiver, its received optical power is essentially linear with the output voltage. Thus, ω can represent the output voltage.

3. Simulation and Discussion

We set up two color lights (blue and green) to explore the effect of wavelength, changed the concentration of Maalox solution to simulate three kinds of water quality, and chose the quartz lens as the optical antenna of the receiver. The specific parameters are shown in Table 1.

Figure 3 shows the impact of the spatial patterns on the output voltage under three distinct water quality conditions, employing both blue and green lights. Compared to Gaussian beams, Bessel beams show significant robustness in turbid water regardless of the wavelength utilized. In clear seawater with $C_M = 0.3$ mg/L, the output voltage consistently maintains a relative advantage when using Gaussian beams. As turbidity rises, the output voltage when using Bessel beams shows an advantage at longer communication distances and eventually achieves complete overtaking. This is because the scattered photons come from the scattering of the main optical axis beam. The transverse intensity of the Bessel beam remains concentrated along the main optical axis without significant change over the non-diffracting length. This minimizes the interaction of the Bessel beam photons with the particles in the water, thus maintaining the signal light intensity over longer communication distances in the main optical axis. At lower turbidity, the difference in intensity between the Bessel and Gaussian beams on the main optical axis is small. The scattered light intensity of the Bessel beam is lower than that of the Gaussian beam due to weaker scattering. At higher turbidity, the Bessel beam is significantly

Table 1. Parameters of the Simulation.

Parameter	Value
Wavelength λ	450, 520 nm
Concentration of Maalox solution C_M	0.3, 0.7, 3.5 mg/L
The half of the FOV η	10° – 90°
Refractive index of the lens	1.46
Base angle of the lens for the Bessel beams β	$\pi/360$

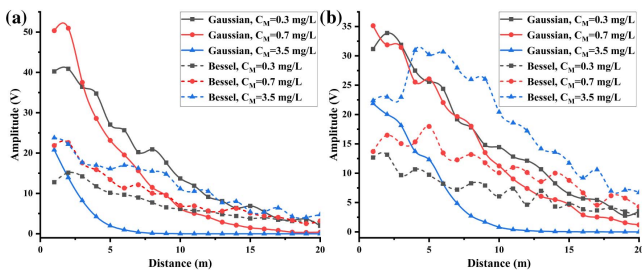


Fig. 3. For (a) $\lambda = 450$ nm and (b) $\lambda = 520$ nm, the output voltages of the MPPC based on the Gaussian beams versus the Bessel beams at different distances.

more intense than the Gaussian beam in the main optical axis, and therefore its scattered light intensity is also higher.

Figure 4 shows the impact of the optical wavelength on the output voltage under three distinct water quality conditions, employing both the Gaussian and Bessel beams. With lower turbidity of the seawater, the seawater absorbs blue light less than green light. Therefore, the output voltage based on blue light is stronger when the communication distance is shorter. As turbidity increases, seawater gradually absorbs blue light more strongly than green light. This causes the scattered light intensity of the blue light to decrease more rapidly, thus making the output voltage based on the blue light weaker than that based on the green light at longer communication distances. From Fig. 4(a), as the turbidity of seawater increases, the output voltage decreases and decays faster. This reflects that the Gaussian beam is more sensitive to the seawater absorption. From Fig. 4(b), the output voltage increases as the seawater turbidity increases due to stronger scattering compensating for absorption. This reflects that Bessel beams are more sensitive to the seawater scattering.

Insights derived from our previous analyses provide practical guidelines for selecting emitter optical wavelengths and spatial modes appropriate for specific environmental conditions and communication targets. When the seawater is clearer or the communication distance is shorter, the blue light and Gaussian beams can be preferred. On the contrary, the green light and Bessel beams can be preferred.

Figure 5 shows the gain that can be achieved for different FOV cases at communication distances $D = 1$ m and $D = 11$ m after using an optical lens with a refractive index of 1.46 as an antenna. As shown in Figs. 5(a)–5(c), the power gain at various water quality conditions and optical wavelengths utilizing the lens is greater than 0 at shorter communication distances. As shown in Figs. 5(b)–5(d), in the case of a large communication distance, a gain of less than 0 occurs with the use of a lens. Therefore, in pursuit of power gain from a larger equivalent photosensitive area, it is necessary to explore new antenna design methods or employ array combinations.

4. Experiment and Results

To confirm the accuracy of the model, experiments were conducted in a controlled laboratory environment using a water

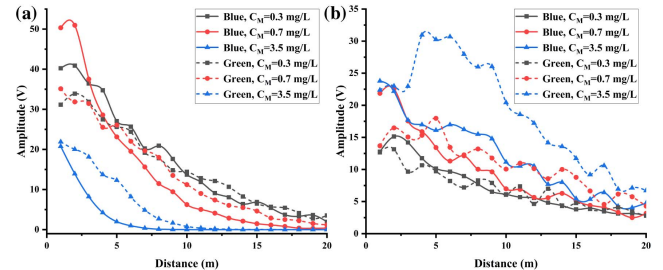


Fig. 4. Output voltages based on (a) Gaussian and (b) Bessel beams for three water quality cases and two wavelength cases ($\lambda = 450, 520$ nm).

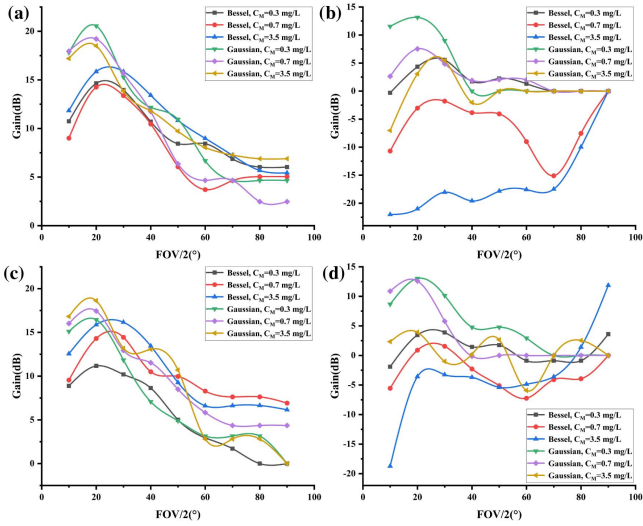


Fig. 5. Power gains obtained at different half angles of the FOV after using the lens ($n = 1.46$) for (a) $D = 1$ m, $\lambda = 450$ nm, (b) $D = 11$ m, $\lambda = 450$ nm, (c) $D = 1$ m, $\lambda = 520$ nm, and (d) $D = 11$ m, $\lambda = 520$ nm.

tank. As shown in Fig. 6, the experimental setup consisted of a transmitter (including a laser and a lens with an optical power of 50 mW), a receiver (MPPC with a photoelectric sensitivity of 1×10^8 V/W), and a water tank. The water tank, measuring length 1.5 m \times width 0.5 m \times height 0.5 m, had walls covered with black material to minimize reflective interference. The transmitter is located at one end and emits a beam perpendicular to the glass surface, while the receiver is located at a designated narrow window on the front of the water tank.

Figure 7 shows the output voltages of three water quality conditions based on 450 and 520 nm lasers in a closed environment obtained from experimental measurements and simulations. The output voltage based on the blue light is higher than that based on the green light at lower impurity concentrations. As water turbidity increases, the output voltage difference decreases between the outputs based on the two wavelengths. When $C_M = 3.5$ mg/L, the output voltage based on the green light exceeds that based on the blue light. This corresponds to the performance of Fig. 4 in the previous section. The simulation results obtained after incorporating the reflection factor of the enclosed environment into the model exhibit an excellent degree of consistency with the experimental data, as corroborated by an R -squared value nearing 0.99.

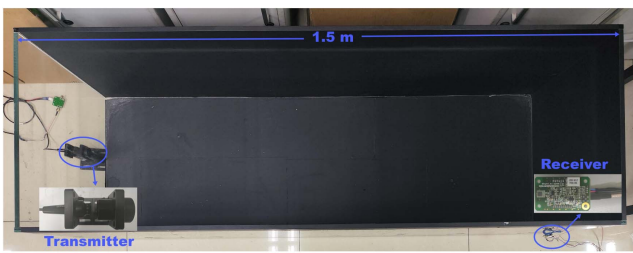


Fig. 6. Experimental scenario diagram.

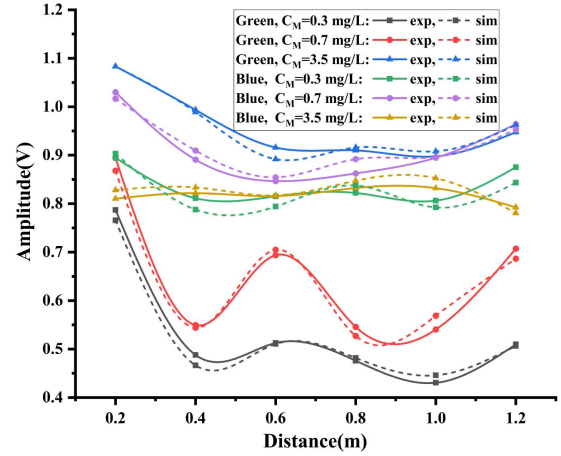


Fig. 7. Output voltages based on 450 and 520 nm lasers for three water quality conditions in a closed environment.

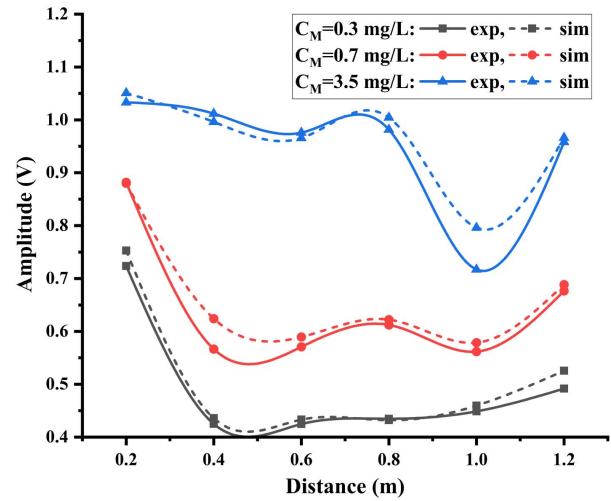


Fig. 8. Output voltages based on 450 nm Bessel beams for three water quality conditions.

The confined environment of the tank results in constant reflection and attenuation of the beam in a finite space, thus blurring the effect of the spatial pattern on the output voltage. However, to confirm the accuracy of the model, simulations were performed to obtain the output voltage based on the blue Bessel beams, which were subsequently compared with the experimental data, as shown in Fig. 8. It is evident that the model fitting agrees well with the empirical results, with an R -squared value of about 0.98.

5. Conclusion

We establish a comprehensive USLC channel model by considering the effect of the transceiver configuration and investigate the effects of the transmitter optical wavelength and spatial pattern, the seawater turbidity, the communication distance, and

the receiver optical antenna on USLC performance. The simulation results indicate that judicious selection of transceiver parameters is essential to maximize the received optical power in different environmental conditions and communication ranges. Specifically, for scenarios with low seawater turbidity and short communication distances, the blue Gaussian beam is recommended due to its strong scattering. Conversely, for scenarios with higher turbidity and longer communication distances, the green Bessel beam is more advantageous due to its resistance to absorption. The receiver optical antenna is suitable for use in short-range USLC, otherwise it will not provide stable gain. These insights promise to provide a foundational reference for future research efforts of USLC to guide the design and selection of transceiver devices for different communication environments.

Acknowledgements

This work was supported by the National Natural Science Foundation of China (No. 62371058) and the Beijing Municipal Natural Science Foundation (No. L232048).

References

1. M. F. Ali, D. N. K. Jayakody, and Y. Li, "Recent trends in underwater visible light communication (UVLC) systems," *IEEE Access* **10**, 22169 (2022).
2. H. Qiu, Z. Huang, J. Xu, *et al.*, "Unified statistical thermocline channel model for underwater wireless optical communication," *Opt. Lett.* **48**, 636 (2023).
3. X. Sun, C. H. Kang, M. Kong, *et al.*, "A review on practical considerations and solutions in underwater wireless optical communication," *J. Lightwave Technol.* **38**, 421 (2020).
4. V. V. Belov, I. Juwiler, N. Blaunstein, *et al.*, "NLOS communication: theory and experiments in the atmosphere and underwater," *Atmosphere* **11**, 1122 (2020).
5. M. Sait, X. Sun, O. Alkhazragi, *et al.*, "The effect of turbulence on NLOS underwater wireless optical communication channels [Invited]," *Chin. Opt. Lett.* **17**, 100013 (2019).
6. M. Sait, Y. Guo, O. Alkhazragi, *et al.*, "The impact of vertical salinity gradient on non-line-of-sight underwater optical wireless communication," *IEEE Photonics J.* **13**, 7300609 (2021).
7. X. Sun, W. Cai, O. Alkhazragi, *et al.*, "375-nm ultraviolet-laser based non-line-of-sight underwater optical communication," *Opt. Express* **26**, 12870 (2018).
8. A. A. B. Umar, M. S. Leeson, and I. Abdullahi, "Modelling impulse response for NLOS underwater optical wireless communications," in *2019 15th International Conference on Electronics, Computer and Computation (ICECCO)* (2019).
9. R. Boluda-Ruiz, P. Rico-Pinazo, B. Castillo-Vazquez, *et al.*, "Impulse response modeling of underwater optical scattering channels for wireless communication," *IEEE Photonics J.* **12**, 7904414 (2020).
10. Y. Zhao, A. Wang, Z. Long, *et al.*, "Performance evaluation of underwater optical communications using spatial modes subjected to bubbles and obstructions," *Opt. Lett.* **42**, 4699 (2017).
11. X. He, M. Li, and L. Rao, "Underwater Bessel-like beams with enlarged depth of focus based on fiber microaxicon," *Chin. Opt. Lett.* **20**, 072601 (2022).
12. A. Laux, R. Billmers, L. Mullen, *et al.*, "The a, b, c s of oceanographic lidar predictions: a significant step toward closing the loop between theory and experiment," *Optica Acta Int. J. Opt.* **49**, 439 (2002).
13. T. J. Petzold, Volume scattering functions for selected ocean waters (Scripts Inst. Oceanogr. Report SIO, 1972).
14. F. Hu, *Theoretical study on the influence of water characteristic parameters on the propagation characteristics of Gaussian beam* (Nanchang Hangkong University, 2021).
15. V. I. Haltrin, "Chlorophyll-based model of seawater optical properties," *Appl. Opt.* **38**, 6826 (1999).
16. Y. Zhang, Y. Wang, and A. Huang, "Analysis of underwater laser transmission characteristics under Monte Carlo simulation," in *2018 OCEANS—MTS/IEEE Kobe Techno-Oceans (OTO)* (2018).
17. L. Wang, S. L. Jacques, and L. Zheng, "MCML—Monte Carlo modeling of light transport in multi-layered tissues," *Comput. Methods Prog. Biomed.* **47**, 131 (1995).
18. P. P. Manousiadis, S. Rajbhandari, R. Mulyawan, *et al.*, "Wide field-of-view fluorescent antenna for visible light communications beyond the étendue limit," *Optica* **3**, 702 (2016).